World Academy of Science, Engineering and Technology
International Journal of Mechanical and Mechatronics Engineering
Vol:11, No:2, 2017

Numerical Simulations of Acoustic Imaging in Hydrodynamic Tunnel with Model Adaptation and Boundary Layer Noise Reduction

Sylvain Amailland, Jean-Hugh Thomas, Charles Pézerat, Romuald Boucheron, Jean-Claude Pascal

***Abstract*—**The noise requirements for naval and research vessels have seen an increasing demand for quieter ships in order to fulfil current regulations and to reduce the effects on marine life. Hence, new methods dedicated to the characterization of propeller noise, which is the main source of noise in the far-field, are needed. The study of cavitating propellers in closed-section is interesting for analyzing hydrodynamic performance but could involve significant difficulties for hydroacoustic study, especially due to reverberation and boundary layer noise in the tunnel. The aim of this paper is to present a numerical methodology for the identification of hydroacoustic sources on marine propellers using hydrophone arrays in a large hydrodynamic tunnel. The main difficulties are linked to the reverberation of the tunnel and the boundary layer noise that strongly reduce the signal-to-noise ratio. In this paper it is proposed to estimate the reflection coefficients using an inverse method and some reference transfer functions measured in the tunnel. This approach allows to reduce the uncertainties of the propagation model used in the inverse problem. In order to reduce the boundary layer noise, a cleaning algorithm taking advantage of the low rank and sparse structure of the cross-spectrum matrices of the acoustic and the boundary layer noise is presented. This approach allows to recover the acoustic signal even well under the boundary layer noise. The improvement brought by this method is visible on acoustic maps resulting from beamforming and DAMAS algorithms.

***Keywords*—**Acoustic imaging, boundary layer noise denoising, inverse problems, model adaptation.

I. Introduction

THE acoustic imaging techniques in aero/hydrodynamic tunnel have seen an increasing of popularity and performance over the last few decades. The delay-and-sum beamforming in the frequency domain is widely used in acoustic tunnels due to the robustness of this approach. Unfortunately this technique involves side-lobe effects that strongly reduce the acoustic imaging performance especially in low frequencies.

Several methods such as DAMAS [1] (Deconvolution Approach for the Acoustic Mapping of Acoustic Sources), CLEAN-SC (Source Coherence) [2] have been proposed to remove the side-lobe effect and then increase the spatial resolution. Classically, the free field propagation model is used for the characterisation of acoustic source in closed wind tunnel [3], [4]. However, the relevance of the results depends on the accuracy of the propagation model used in the imaging technique.

S. Amailland, J.-H. Thomas, C. Pézerat, and J.-C. Pascal are with the Laboratoire d'Acoustique de l'Université du Maine (LAUM UMR CNRS 6613), Le Mans, France (e-mail: sylvain.amailland@univ-lemans.fr, jean-hugh.thomas@univ-lemans.fr, charles.pezerat@univ-lemans.fr, Jean-Claude.Pascal@univ-lemans.fr).

Fenech et al. [5] propose to use the image source method (ISM) in order to take into consideration the reflections in the tunnel. Recently, Fischer et al. [6] have introduced an empirical de-reverberation method based on measured Green's functions. They show that the source position is exactly recovered for a wide frequency range but only when it matches one of the positions used to measure the Green's functions.

The performance of the localisation techniques can be strongly affected by the boundary layer noise. Blacodon [7] proposes a denoising method based on noise reference. However, the efficiency of this noise removal process depends on the accuracy of the noise signal. Hence, the variations between the estimated noise spectrum and the actual noise could lead to strong errors.

In this paper, a numerical methodology for the identification of acoustic sources in the hydrodynamic tunnel using hydrophone array corrupted by boundary layer noise is presented. Firstly it is proposed to estimate the reflection coefficients using an inverse method and some reference transfer functions in order to reduce the uncertainties about the propagation model. Secondly a denoising method that does not need the cross-spectrum estimation of the noise is presented. This approach takes advantage of the low rank and sparse structure of the cross-spectrum matrices of the acoustic and the boundary layer noise and is based on the RPCA (Robust principal component analysis) algorithm [8].

II. Acoustic Propagation

A. Source Image Theory

The acoustic field $p(\boldsymbol{r})$ at a given position $\boldsymbol{r}$ resulting from a radiating source on a surface $S(\boldsymbol{r}_s)$ is given by

$$p(\boldsymbol{r}) = \int_S i\omega\rho q_s(\boldsymbol{r}_s) G(\boldsymbol{r}|\boldsymbol{r}_s) dS(\boldsymbol{r}_s) + n, \qquad (1)$$

with $q_s(\boldsymbol{r}_s)$ the volume velocity of the source, $G(\boldsymbol{r}|\boldsymbol{r}_s)$ the Green's function of the environment with a density of ρ and n accounts for the measurement noise. The image source method (ISM) is a well known technique to model the acoustic propagation in enclosed space. This approach considers that the boundaries of the enclosed space can be replaced by mirror image sources located outside the enclosed space [5], [9]. Then the acoustic propagation is calculated by summing the contributions of the image sources and the true source. Thus the Green's function between a receiver ($\boldsymbol{r}$) and a source ($\boldsymbol{r}_s$)

can be written as

$$G(\boldsymbol{r}|\boldsymbol{r}_s) = \frac{i\omega\rho}{4\pi}\left[\frac{e^{-ik\|\boldsymbol{r}-\boldsymbol{r}_s\|_2}}{\|\boldsymbol{r}-\boldsymbol{r}_s\|_2} + \sum_{j=1}^{J}\frac{e^{-ik\|\boldsymbol{r}-\boldsymbol{r}_j\|_2}}{\|\boldsymbol{r}-\boldsymbol{r}_j\|_2}R^{O_j}\right], \quad (2)$$

with r_j the position of the j^{th} image source. The reflection coefficient is given by R, and O_j is the order of reflection. The reflection coefficient is supposed to be independent of the frequency and is not angularly variable. In a rectangular enclosure, the image sources can be positioned as in Fig. 1. Their positions directly depend on the true source and the geometry of the enclosed space.

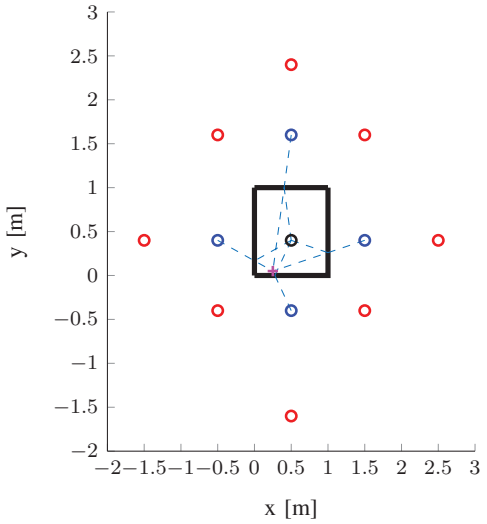

Fig. 1 Image source positions for a square tunnel ▬: acoustic source (O), image sources order 1 (O), image sources order 2 (O), receiver (+) and reflection path - - -

In many cases, the boundary conditions are difficult to know and the reflection coefficients are not well estimated. Therefore that involves inaccurate results in the Green's function calculation.

B. Reflection Coefficient Estimation

In this paper, it is proposed to estimate the reflection coefficients ($\boldsymbol{R}$) using an inverse method and some reference transfer functions ($\boldsymbol{G}_{ref}$). The system of linear equations can be written as

$$\boldsymbol{G}_{ref} = \boldsymbol{G}_{dir} + \boldsymbol{A}_{ima}\boldsymbol{R} + \boldsymbol{n}, \quad (3)$$

with $\boldsymbol{G}_{dir}$ the transfer function of the direct field due to the true source propagation in free field and $\boldsymbol{n}$, the noise which follows a complex Gaussian distribution $\boldsymbol{n} \sim \mathcal{CN}\left(0, \sigma^2\boldsymbol{I}\right)$. The transfer functions, between the array and a given point on the focal plane, Fig. 2 is obtained using a known source. The matrix $\boldsymbol{G}_{dir}$ is supposed to be known and (3) can be rewritten as

$$\boldsymbol{G}_{ref} - \boldsymbol{G}_{dir} = \boldsymbol{A}_{ima}\boldsymbol{R} + \boldsymbol{n} = \boldsymbol{B}. \quad (4)$$

It must be noted that the positions for the estimation of the reference transfer functions are randomly chosen. The aim of this work is to estimate the reflection coefficients by solving

$$\tilde{\boldsymbol{R}}_\lambda = \underbrace{\text{Argmin}}_{\boldsymbol{R}}\{\| \tilde{\boldsymbol{B}} - \boldsymbol{A}_{ima}\boldsymbol{R} \|_2^2 + \lambda \| \boldsymbol{L}\boldsymbol{R} \|_p^p\}, \quad (5)$$

with λ and $\boldsymbol{L}$ the regularisation parameter and the regularisation matrix and p defines the *a priori* distribution of $\boldsymbol{L}\boldsymbol{R}$. In most cases, inverse problems are not well-posed and resolution can be tricky. In this work, we propose to introduce the sparse principle ($p = 1$) on the derivative of the reflection coefficients.

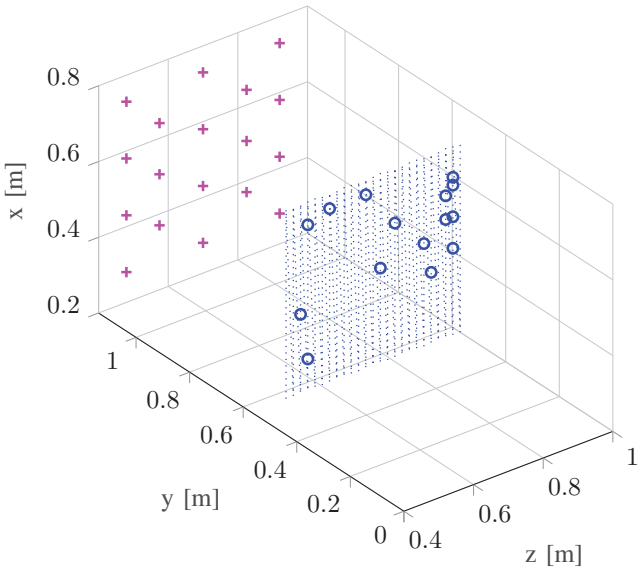

Fig. 2 Hydrophone positions (+), focal plane (·····) and source positions for transfer function estimation (O)

The regularisation matrix based on the first order derivative is proposed in (6). The derivative pattern is organised as a function of the reflection order,

$$\boldsymbol{L} = \begin{bmatrix} -1 & 1 & 0 & 0 & 0 & 0 & 0 & \cdots \\ 0 & -1 & 1 & 0 & 0 & 0 & 0 & \cdots \\ 0 & 0 & -1 & 1 & 0 & 0 & 0 & \cdots \\ 0 & 0 & 0 & 0 & -1 & 1 & 0 & \cdots \\ 0 & 0 & 0 & 0 & 0 & -1 & 1 & \cdots \\ \vdots & \vdots & \vdots & \vdots & \vdots & \vdots & \vdots & \ddots \end{bmatrix} \begin{matrix} \} Order\ 1 \\ \\ \\ \} Order\ 2 \end{matrix}, \quad (6)$$

the matrix $\boldsymbol{L}$ is rectangular and not directly invertible. For such case, Elden [10] proposes to rewrite (5) into the standard formulation,

$$\bar{\tilde{\boldsymbol{R}}}_\lambda = Argmin\{\| \bar{\tilde{\boldsymbol{B}}} - \bar{\boldsymbol{A}}_{ima}\bar{\boldsymbol{R}} \|_2^2 + \lambda \| \bar{\boldsymbol{R}} \|_1^1\}, \quad (7)$$

with $\bar{\cdot}$ denote the matrices or vectors that take into account the regularisation matrix $\boldsymbol{L}$. Equation (7) can be solved using FISTA algorithm [11]. The regularisation parameter is set to $\lambda = 0.01 \| 2\bar{\boldsymbol{A}}_{ima}^H\bar{\boldsymbol{b}} \|_\infty$ according to [12]. Fig. 3 shows the reflection coefficients as a function of the reflection order.

The influence of the reflection coefficients identification is visible in Fig. 4. Thus, the uncertainties about the propagation model can be reduced.

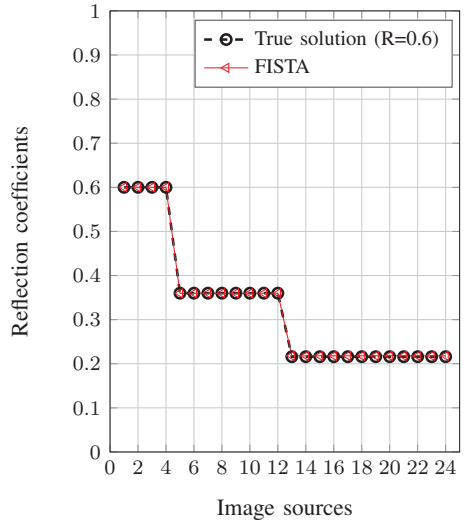

Fig. 3 Reflection coefficients (order 3) at 5 kHz, using 15 transfer functions with SNR = 40 dB

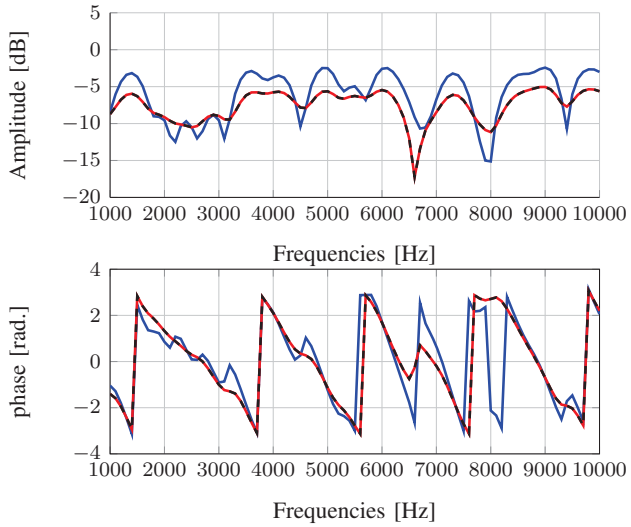

Fig. 4 Propagation model: wrong model R=1 (——), true model R=0.6 (——) and optimised model (- - -)

III. Boundary Layer Noise Reduction

This section deals with boundary layer noise reduction. The water flow in the tunnel involves strong pressure fluctuation on the tunnel wall due to the development of a turbulent boundary layer noise. Such noise can become very problematic for the characterisation of acoustic sources lower than the flow. In this part, we use semi-empirical models, based on Corcos' and Goody's studies, to simulate the flow noise and a denoising algorithm based on low rank and sparse decomposition of the cross-spectrum matrix.

A. Boundary Layer Noise Modeling

The boundary layer involves a wall-pressure that could be separated in two parts [13]:

- Convective: Pressure due to the turbulences on the wall,
- Acoustic: Sound pressure radiated by the turbulences.

These two parts are relatively well separated in the wave number domain, Fig. 5. The higher pressure fluctuation is located on the convective region, centred on $k_1 = \omega/U_c$ (high wave number), whereas the acoustic part takes place in the low wave numbers ($k = \omega/c$).

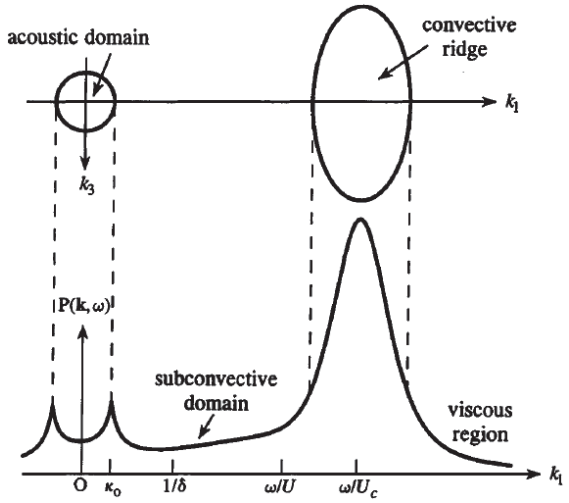

Fig. 5 Turbulent boundary layer spectrum in the wavenumber domain and at low mach number ($\omega\delta/U$) [14]

The wall pressure field is simulated using semi-empirical methods such as Corcos and Goody models. The aim of this part is not to describe accurately the wall-pressure but rather to see the influence of such noise on the sound pressure.

Goody's model describes the energetic distribution of the boundary layer noise as a function of the frequency, and is given by

$$S_{nn}(\omega) = \frac{3\tau_\omega^2 \delta \left(\frac{\omega\delta}{U}\right)^2}{U\left(\left[0.5 + \left(\frac{\omega\delta}{U}\right)^{0.75}\right]^{3.7} + \left[1.1 R_T^{-0.57}\left(\frac{\omega\delta}{U}\right)\right]^7\right)}, \tag{8}$$

with $R_T = \frac{u_\tau^2 \delta}{\nu U}$ the Reynolds number [15]. Table I shows the boundary layer parameters in water flow.

TABLE I
Water Flow Parameters at 16°C [16]

Parameters	Values
Fluid velocity	$U = 10\ m/s$
Fluid density	$\rho = 1000\ kg/m^3$
Convection velocity	$U_c = 0.8\ U$
Boundary layer thickness	$\delta = 0.047\ m$
Friction velocity	$u_\tau = 0.16\ m/s$
Kinematic viscosity	$\nu = 1.1 \cdot 10^{-6}\ m^2/s$
Shear stress	$\tau_\omega = 3\ N/m^2$

The spatial coherence inside the wall-pressure is described using Corcos model [17],

$$G_{nn}(r_x, r_z, \omega) = S_{nn}(\omega)\left(e^{-\omega\alpha_x \frac{|r_x|}{U_c}} e^{-\omega\alpha_z \frac{|r_z|}{U_c}} e^{-j\omega \frac{r_z}{U_c}}\right), \tag{9}$$

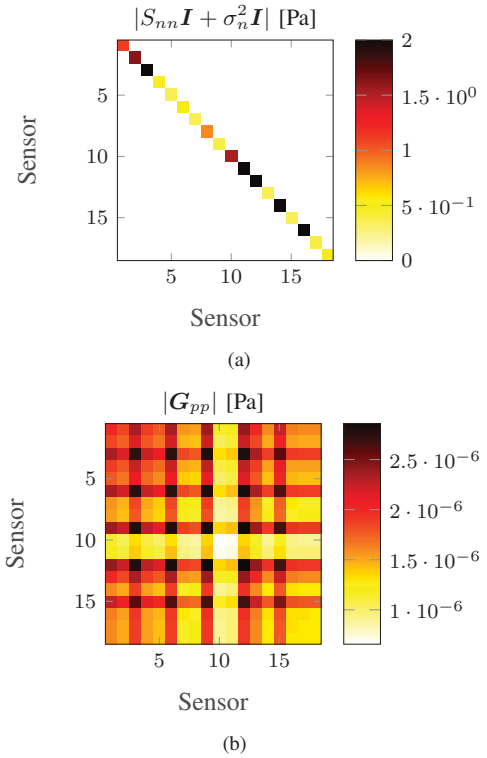

Fig. 6 Typical cross-spectrum matrices for spatially decorrelated noise: noise part (a), acoustic part (b)

with r_x and r_z the distances between sensors, in the xz plane, α_x and α_z the spatial coherence rates. The correlation lengths are strongly smaller than the distance between sensors, thus the sound field can be viewed as a decorrelated sound pressure. The total wall-pressure can be written in terms of the cross-spectrum matrix,

$$\hat{\boldsymbol{G}}_{pp}(\omega) = \underbrace{\boldsymbol{G}_{pp}(\omega)}_{\text{Acoustic propagation}} + \underbrace{S_{nn}(\omega)\boldsymbol{I}}_{\text{Boundary layer noise}} + \underbrace{\sigma_n^2(\omega)\boldsymbol{I}}_{\text{Noise measurement}}, \tag{10}$$

with $\boldsymbol{I}$ the identity matrix, and σ_n^2 the noise variance which follows a Gaussian distribution and could be written as a function of the signal-to-noise ratio SNR $_n$,

$$\sigma_n^2 = 10^{-SNR_n 0.1} max(diag(\boldsymbol{G}_{pp}(\omega) + S_{nn}(\omega)\boldsymbol{I})). \tag{11}$$

B. Sparse Low Rank Decomposition

In this subsection, a denoising method based on cross-spectrum matrix decomposition is developed. Indeed, the wall-pressure field can be separated into an acoustic part ($\boldsymbol{Q}(\omega)$) supposed to be of low rank and a boundary layer noise part ($\boldsymbol{D}(\omega)$) assumed to be sparse (diagonal),

$$\hat{\boldsymbol{G}}_{pp}(\omega) = \boldsymbol{Q}(\omega) + \boldsymbol{D}(\omega). \tag{12}$$

The method presented in the following is based on the robust principal component analysis and allows to jointly estimate the acoustic and the noise parts in case of a spatially decorrelated wall-pressure field.

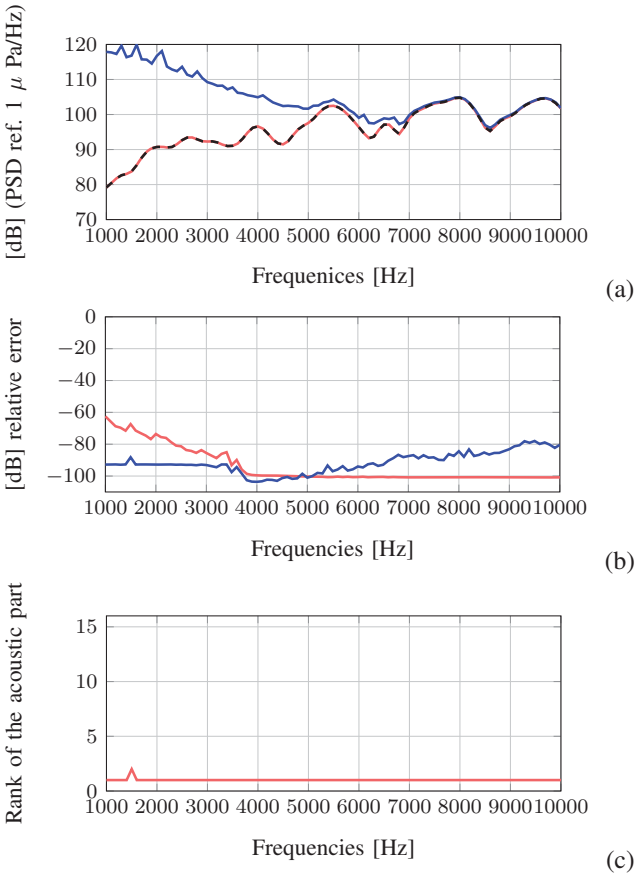

Fig. 7 Results of the denoising method: (a) acoustic PSD (——), total wall-pressure PSD (——) and denoised PSD (- - -). (b) Relative error on the acoustic part (——) and the noise part (——). (c) Estimation of the rank of the acoustic part(——) SNR$_n$ = -5 dB

$$(\hat{\boldsymbol{Q}}(\omega), \hat{\boldsymbol{D}}(\omega)) = \underbrace{Argmin}_{\boldsymbol{Q},\boldsymbol{D}}\{\|\boldsymbol{Q}(\omega)\|_* + \lambda\|\boldsymbol{D}(\omega)\|_1\}, \quad \text{under constraint } \hat{\boldsymbol{G}}_{pp}(\omega) = \boldsymbol{Q}(\omega) + \boldsymbol{D}(\omega), \tag{13}$$

with $\|\boldsymbol{Q}(\omega)\|_*$ the nuclear norm of $\boldsymbol{Q}(\omega)$ and λ the regularisation parameter. Wright et al. proposed to solve the problem using accelerated proximal gradient and set $\lambda = m^{-1/2}$ with m the number of rows [8]. Fig. 6 illustrates the cross-spectrum matrix of the acoustic and the boundary layer noise parts. Fig. 7 shows the efficiency of the boundary layer noise reduction. Indeed, the RPCA algorithm estimates precisely the acoustic part even when the signal-to-noise ratio is equal to -5 dB.

IV. Acoustic Imaging

A. Beamforming

The beamforming method (delay and sum) is a robust method largely used in aeroacoustic studies [5], [1]. In the frequency domain, this technique can be viewed as a spatial filter that estimates the power spectrum density (PSD) $\tilde{Y}_i(\omega)$ at a given focal point i

$$\tilde{Y}_i(\omega) = \boldsymbol{w}_i^H(\omega)\hat{\boldsymbol{Q}}(\omega)\boldsymbol{w}_i(\omega), \tag{14}$$

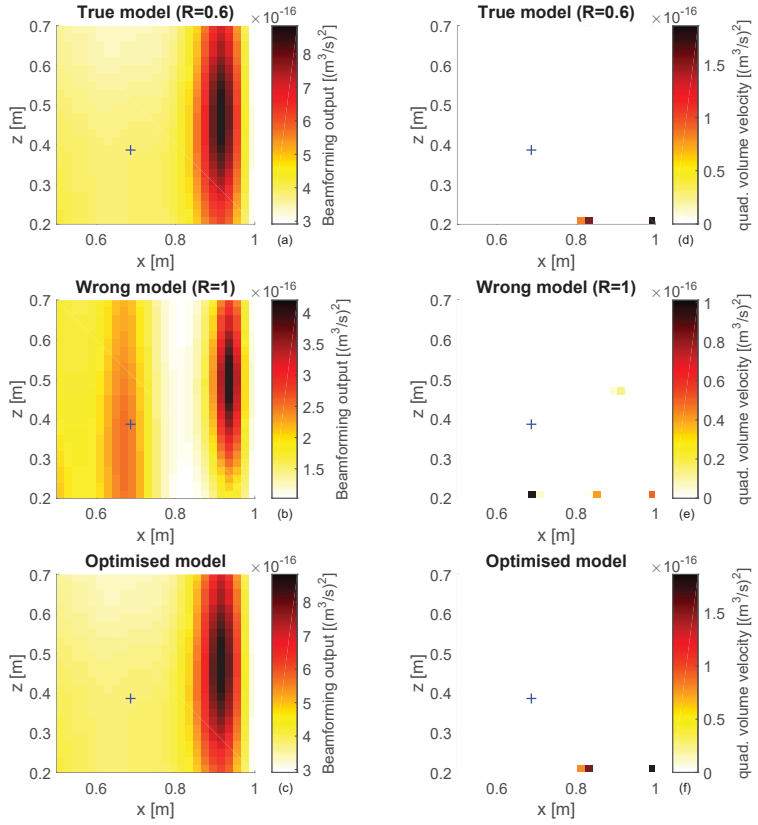

Fig. 8 Acoustic imaging results for a monopolar source without denoising step, beamforming: (a) true model, (b) wrong model, (c) optimised model and DAMAS: (d) true model, (e) wrong model, (f) optimised model, at 3 kHz

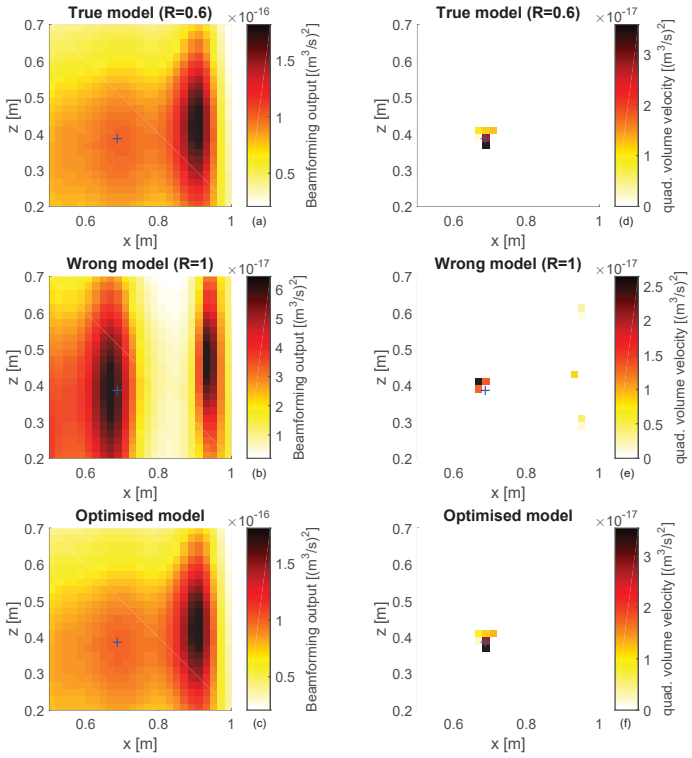

Fig. 9 Acoustic imaging results for a monopolar source with denoising step, beamforming: (a) true model, (b) wrong model, (c) optimised model and DAMAS: (d) true model, (e) wrong model, (f) optimised model, at 3 kHz

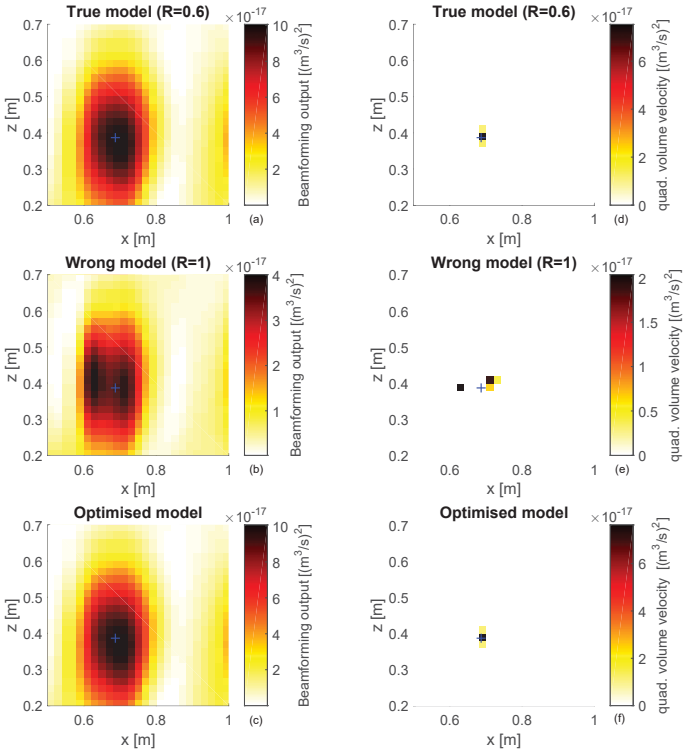

Fig. 10 Acoustic imaging results for a monopolar source with denoising step, beamforming: (a) true model, (b) wrong model, (c) optimised model and DAMAS: (d) true model, (e) wrong model, (f) optimised model, at 5 kHz

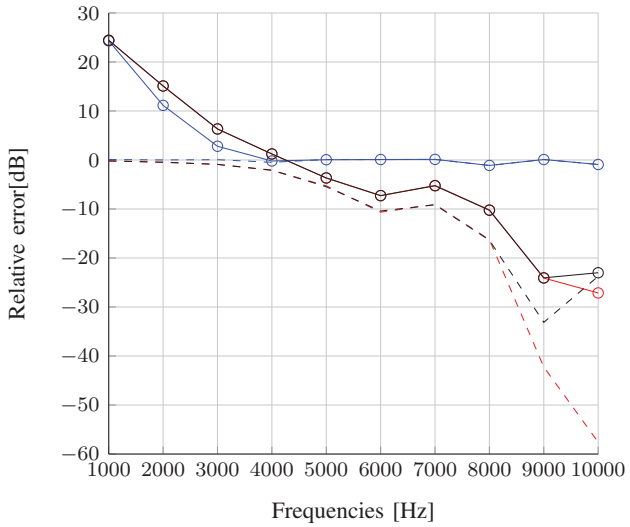

Fig. 11 Relative error on the source strength reconstruction. Without denoising: true model (—o—), wrong model (—o—), optimised model (—o—). With denoising method: true model (- - -), wrong model (- - -), optimised model (- - -)

with $\boldsymbol{w}_i(\omega)$ the steering vector based on the propagation model and $\boldsymbol{g}_i(\omega)$ the transfer function vector between the array and the focal point i

$$w_i(\omega) = \frac{\boldsymbol{g}_i(\omega)}{\boldsymbol{g}_i^H(\omega)\boldsymbol{g}_i(\omega)}. \tag{15}$$

The acoustic sources are supposed to be decorrelated, then the beamforming output can be rewritten as

$$\begin{aligned}\tilde{Y}_i(\omega) &= \boldsymbol{w}_i^H(\omega)\sum_{q=1}^{N} x_q(\omega)\boldsymbol{g}_q(\omega)\boldsymbol{g}_q^H(\omega)\boldsymbol{w}_i(\omega) + (\sigma_n^2)\frac{1}{\|\boldsymbol{g}_i(\omega)\|^2},\\ &= \sum_{q=1}^{N} A_{i,q}(\omega)x_q(\omega) + (\sigma_n^2)\frac{1}{\|\boldsymbol{g}_i(\omega)\|^2},\end{aligned} \tag{16}$$

with N the number of decorrelated sources, $x_q(\omega)$ the source strength at the focal point q and $\boldsymbol{A}(\omega)$ the array response.

B. Deconvolution

The beamforming results suffer from low spatial resolution in low frequencies. In order to enhance the acoustic maps Brooks et al. [1] propose the DAMAS algorithm. This deconvolution algorithm allows to reduce the side-lobe effects and to estimate the source strength $\boldsymbol{X}$ by solving [1]

$$\tilde{\boldsymbol{Y}}(\omega) = \boldsymbol{A}(\omega)\boldsymbol{X}(\omega), \tag{17}$$

with $\tilde{\boldsymbol{Y}}(\omega)$ the beamforming output, $\boldsymbol{A}(\omega)$ the array response and $\boldsymbol{X}(\omega)$ the source strength. The solution at iteration n is given by

$$\hat{x}_q^{(n)} = max\left\{0, \left(\tilde{Y}_q - \sum_{k=1}^{q-1} A_{q,k}x_k^{(n)} - \sum_{k=q+1}^{N} A_{q,k}x_k^{(n-1)}\right)\right\}. \tag{18}$$

Fig. 8 shows the effects of the boundary layer noise on the beamforming and the DAMAS results for the different

propagation models in the case of one monopolar source without the denoising step, whereas Fig. 9 illustrates the acoustic maps after the denoising process.

Through these simulations, the noise due to the boundary layer introduces strong artefacts on the DAMAS maps. The denoising step allows to reduce the influence of the noise and therefore improves the results. Moreover, it is clear that working with a propagation model that is not perfect can involve important errors on the acoustic maps, Fig. 10. Thanks to the reference transfer functions, the uncertainties on the model are reduced which lead to an improvement of the acoustic maps. According to Fig. 9 and 10 we can see that the introduction of Green function which takes into account reflections, introduced strong side lobes that can be higher than de main lobe.

Fig. 11 displays the relative error as a function of the frequency defined as

$$Error(\omega) = 10\log_{10}\left(\frac{\parallel \tilde{\boldsymbol{X}}(\omega) - \boldsymbol{X}(\omega) \parallel_2}{\parallel \boldsymbol{X}(\omega) \parallel_2}\right), \qquad (19)$$

with $\boldsymbol{X}(\omega)$ the true solution and $\tilde{\boldsymbol{X}}(\omega)$ the solution after deconvolution, and reduction or not of the boundary layer noise. According to Fig. 11, the errors in the propagation model involve large artefacts over all the frequencies. The identification of the reflection coefficients improves the acoustic map results. Indeed, after 5 kHz the errors are below -10 dB which means that the results are accurate in terms of source localisation and quantification. The poor results in low frequencies are due to the fact that the DAMAS algorithm has not yet totally converged and that the solution is a bit spread out. The denoising approach enhances the acoustic map especially in low frequency range.

V. Conclusion

In this paper, an adaptation method capable of reducing the model errors using reference transfer functions is presented. This approach allows the identification of the reflection coefficients associated to the image sources in a closed tunnel and improves our knowledge about the propagation model. In addition, a denoising algorithm for wall-pressure noise is proposed. This method is based on the RPCA algorithm that separates the acoustic signal from the boundary layer noise thanks to the low rank and sparse properties of the cross-spectrum matrices of the acoustic and the boundary layer noise. The improvement brought by these methods enhances the acoustic maps in terms of source localisation and quantification.

Acknowledgment

This research project is funded by the DGA/MRIS

References

[1] T. F. Brooks and W. Humphreys, "A deconvolution approach for the mapping of acoustic sources (DAMAS) determined from phased microphone arrays," *Journal of Sound and Vibration*, vol. 294, no. 4–5, pp. 856 – 879, 2006.

[2] P. Sijtsma, "Clean based on spatial source coherence," *International journal of aeroacoustics*, vol. 6, no. 4, pp. 357–374, 2007.

[3] V. Fleury and R. Davy, "Beamforming-based noise level measurements in hard-wall closed-section wind tunnels," in *Proceedings of the 18th AIAA/CEAS Aeroacoustics Conference*, 2012, pp. 1–22.

[4] L. Koop and K. Ehrenfried, "Microphone-array processing for wind-tunnel measurements with strong background noise. 14th aiaa/ceas aeroacoustics conference, Vancouver, BC, Canada," AIAA-2008-2907, Tech. Rep., 2008.

[5] B. Fenech, "Accurate aeroacoustic measurements in closed-section hard-walled wind tunnels," Ph.D. dissertation, University of Southampton, 2009.

[6] C. J. Fischer, Jeoffrey R. Doolan, "An empirical de-reverberation technique for closed-section wind tunnel beamforming," *American Institute of Aeronautics and Astronautics 22nd AIAA/CEAS Aeroacoustics Conference, Lyon, France*, 2016.

[7] D. Blacodon, "Spectral estimation method for noisy data using a noise reference," *Applied Acoustics*, vol. 72, no. 1, pp. 11 – 21, 2011.

[8] J. Wright, A. Ganesh, S. Rao, Y. Peng, and Y. Ma, "Robust principal component analysis: Exact recovery of corrupted low-rank matrices via convex optimization," in *Advances in neural information processing systems*, 2009, pp. 2080–2088.

[9] H. Kuttruff, *Room acoustics*. Crc Press, 2009.

[10] L. Eldén, "Algorithms for the regularization of ill-conditioned least squares problems," *BIT Numerical Mathematics*, vol. 17, no. 2, pp. 134–145, 1977.

[11] A. Beck and M. Teboulle, "A fast iterative shrinkage-thresholding algorithm for linear inverse problems," *SIAM J. Img. Sci.*, vol. 2, no. 1, pp. 183–202, Mar. 2009.

[12] Z. Lingling, W. Huaxiang, X. Yanbin, and W. Da, "A fast iterative shrinkage-thresholding algorithm for electrical resistance tomography," *WSEAS Transactions on Circuits and Systems*, vol. 10, no. 11, pp. 393–402, 2011.

[13] M. Bull, "Wall-pressure fluctuations beneath turbulent boundary laers: some reflections on forty years of research," *Journal of Sound and Vibration*, vol. 190, no. 3, pp. 299 – 315, 1996.

[14] M. Howe, *Acoustics of fluid-structure interactions*. Cambridge university press, 1998.

[15] M. Goody, "An Empirical Spectral Model of Surface-Pressure Fluctuations That Includes Reynolds Number Effects," *American Institute of Aeronautics and Astronautics*, 2002.

[16] M. Aucejo, "Vibro-acoustique des structures immergées sous écoulement turbulent," Ph.D. dissertation, INSA de Lyon, 2010.

[17] Y. Hwang, W. Bonness, and S. Hambric, "On modeling structural excitations by low speed turbulent boundary layer flows," DTIC Document, Tech. Rep., 2003.